ISA Transactions 135 (2023) 551–566

Contents lists available at ScienceDirect

ISA Transactions

journal homepage: www.elsevier.com/locate/isatrans

Practice article

An improved first-principle model of AC powered solenoid operated valves for maintenance applications

Georges Tod [a], Agusmian Partogi Ompusunggu [b,*], Erik Hostens [c]

[a] CRI Research, Université de Paris, 8bis Rue Charles V, 75004, Paris, France
[b] Centre for Life-Cycle Engineering and Management (CLEM), School of Aerospace, Transport and Manufacturing (SATM), Cranfield University, Bedfordshire, MK43 0AL, UK
[c] Flanders Make vzw, Gaston Geenslaan 8, Heverlee (Leuven), B-3001, Belgium

ARTICLE INFO

Article history:
Received 12 November 2021
Received in revised form 21 September 2022
Accepted 21 September 2022
Available online 27 September 2022

Keywords:
AC solenoid operated valves
Accelerated life test
Wear
Shading ring
Condition monitoring
Magneto-mechanical modelling

ABSTRACT

Solenoid operated valves (SOVs) are critical components in many industrial applications. There has been a continuing interest in the industry to have robust condition monitoring, prognostics and health management tools to support the condition based maintenance and predictive maintenance program for such valves. For critical assets like SOVs, it is of paramount interest to understand why a component might be declared as defective. In such a situation, a first principle-model based approach will always be preferred to a purely data-driven approach, because of its inherent interpretability. Furthermore, first principle-models typically have less free parameters than their data driven counterparts and will require less data to identify their parameters. In this paper, we present the improvement of a first-principle model of alternating current (AC) powered SOVs taking into account two important degradation effects. Using this model, we show that the state of degradation can be estimated from current and input voltage measurement signals on the solenoids. Our method is validated using data from an accelerated life test campaign on 48 identical AC-powered SOVs.

1. Introduction

Since the start of the Industrie 4.0 era, there has been pressure in the industry to transform their maintenance strategy from the traditional corrective/ preventive maintenance strategy to a more advanced Condition Based Maintenance (CBM) or Predictive Maintenance (PdM) strategy [1]. However, the implementation of such an advanced CBM or PdM strategy requires technologies like Condition Monitoring (CM), and Prognostics and Health Management (PHM) of critical assets. These technologies comprise sensing, data acquisition, condition indicator (CI) construction, health assessment, and remaining useful life (RUL) prediction. Due to the wide usage of rotating machinery in the industry, many efforts have been spent since the last few decades to develop CM/ PHM technologies for critical rotating machine components, such as bearings, gears [2]. Among others, solenoid-operated valves (SOVs), which are the focus of this paper, are critical non-rotating machine components widely used in many industrial applications. Therefore, these components also need attention for relevant CM/ PHM technologies development.

SOVs are electrically activated valves, typically used to control the flow or direction of air or liquid in pneumatic or hydraulic power systems. To achieve this functionality, an electrical current is passed through a winding wire, thus generating a magnetic field as schematically illustrated in Fig. 1. At the rest position x_i, the plunger closes the orifice such that the pressurised air coming from the inlet port is not allowed to flow through the outlet port. In this situation, the air flows out through the vent hole instead. As soon as the coil is energised, the current increases, thus causing the electromagnetic force on the plunger to increase. Eventually, the electromagnetic force becomes strong enough to overcome the spring force and the friction force on the plunger so that the plunger moves from the rest position x_i to the end-of-travel position x_e. During the plunger movement, the orifice is opened thus allowing the air to flow out through the outlet port. At the same time, the air flow through the vent hole is gradually decreasing and it stops when the plunger has reached the end-of-travel position x_e.

Depending on the design, an SOV can be either powered by a direct current (DC) or an alternating current (AC) supply. From the usage point of view, SOVs available on the market can be classified into three categories [3], comprising: (1) normally open in comparison with normally closed; (2) direct acting in comparison with pilot controlled; and (3) two way in comparison with three way in comparison with four way. Normally open (closed) is an SOV where the inlet port is open (closed) when the valve is de-energised. A direct acting SOV refers to the one

* Corresponding author.
E-mail address: agusmian.ompusunggu@cranfield.ac.uk (A.P. Ompusunggu).

https://doi.org/10.1016/j.isatra.2022.09.032

Nomenclature

Abbreviation

AC	Alternating Current
ALT	Accelerated Life Test
CBM	Condition Based Maintenance
CI	Condition Indicator
CM	Condition Monitoring
DC	Direct Current
EOL	End of Useful Life
ML	Machine Learning
ODE	Ordinary Differential Equation
PdM	Predictive Maintenance
PHM	Prognostics and Health Management
RUL	Remaining Useful Life
SOV	Solenoid Operated Valve

List of Symbols

$\ddot{x}$	Plunger's acceleration [m/s^2]
$\dot{x}$	Plunger's velocity [m/s]
μ_0	Air permeability [H/m]
c	Viscous damping coefficient [Ns/m]
F_{pt}	Return spring pretension force [N]
F_{dc_0}	The kinetic Coulomb friction force [N]
F_{sh_0}	The shading ring force [N]
k	Return spring stiffness [N/m]
L	Inductance [H]
$l_{\text{air}_{ax,0}}$	Maximal axial air gap [mm]
l_h	Housing length [m]
m	Mass of the plunger [g]
N	Number of main coil winding [–]
R	Coil resistance [Ohm]
r	Residual current error [Ampere]
$V(t)$	Input AC voltage [Volt]
x	Plunger's displacement [m]

where all flow passes through an orifice that is opened directly by an electromagnet and plunger. While a pilot controlled SOV is the one that operates based on a minimum and maximum pressure differential. The pilot controlled SOV make uses of an electromagnet and plunger to open or close a small orifice thus controlling the pressure differential across a piston or diaphragm. A two way SOV has two ports and a single orifice that can be opened or closed. While, a three way SOV consists of three ports and two orifices. A four way SOV has four of five pipe connections, namely one pressure, two cylinder and one or two exhaust. The latter is commonly employed to operate double acting cylinders or actuators. Interested readers are referred to [3] for more descriptions about these different categories.

Such valves are used in a wide range of industrial applications, including the automotive sector, chemical industry, nuclear power plants, etc. [3,4]. Some application examples of SOVs in the automotive industry are for controlling electro-pneumatic braking systems of passenger vehicles and fuel injection systems. While in the nuclear industry, the valves are mainly utilised for safety–critical instrumented functions [4].

In recent years, the awareness of the criticality of SOVs for industrial applications has increased among the CBM/ PdM practitioners and stakeholders, because of some major incidents that investigations attributed to SOV failures [5,6]. One of these catastrophic events that took a lot of public attention is the Transocean Deepwater Horizon disaster in 2010. According to [6], this disaster resulted in 11 people deaths and about 4.9 million barrels of oil spilled into the Gulf of Mexico. To avoid such a catastrophic event and the negative (direct and indirect) impact to the environment, society and human lives, the interest in estimating SOVs health status and their RUL continues to grow in the industry.

1.1. Related works

To the best of the authors' knowledge, early works on CM technologies development for SOVs using a non-invasive method based on the electrical (current and voltage) signals were published around 1990 [4,7,8]. Since then, the development of CM and PHM technologies based on measured electrical signals has been focused on DC-powered SOVs (for example see Refs. [4,8–16]).

Apart from the electrical signals-based method, other non-invasive methods for health estimation of SOVs have also been reported in the literature. Guo et al. [17] developed a fault detection system for SOVs based on vibration sensors. Li et al. [18] developed a method based on a 77 GHz FMCW millimeter-wave radar to measure the plunger displacement of multiple SOVs. In the latter, some condition indicators (CIs) were calculated from the measured plunger displacement signal. The CIs are subsequently used for RUL estimation. However, the non-invasive method using electrical (current and voltage) signals, which are typically available in practice, is preferred because it does not require additional sensors installation.

The crucial steps in the development of CM and PHM technologies for CBM/ PdM applications lie on (1) determining the most effective CIs that represent the degradation processes and failure modes of a component/ asset under investigation and (2) extracting/ computing them from acquired measurement data. Once determined and validated, the CIs can be subsequently used as the input for health assessment, diagnostics and prognostics algorithms. From the literature, three different approaches for the CIs development of SOVs are identified, namely (i) the model-based method, (ii) the data-driven method and (iii) the hybrid method.

In the model-based method, first-principle models are used together with parameter estimation techniques to extract CIs for health assessment and/or predict the RUL of SOVs from measurement data [11,16,19,20]. In this regard, most of the published papers dealt with DC-powered SOVs, where the valve being modelled as an electro-mechanical system [21] is coupled with a fluid system [11,22]. In [23], a high fidelity model using a finite element (FE) approach was developed to predict the stresses, strains and temperature distributions of a solenoid valve.

In the data-driven method, which is physical phenomenon/ model agnostic, raw data or generic/statistical features (as candidates of CIs) computed from the raw data are fed into the machine learning (ML) algorithms for the health assessment and/or RUL prediction of SOVs [12,24,25]. Different techniques, like compressed sensing [26], were also used to compute features from the raw data that can be used as potential candidates of CIs. Instead of using all features, a feature selection algorithm is applied to the features vector to select the most relevant features for the health assessment and RUL prediction of SOVs [15].

In the hybrid approach, a profound understanding of the degradation mechanisms and the manifestation to the SOV dynamic behaviour (e.g. electrical response) is important for the development of a dedicated signal processing method to extract physics-inspired features as CIs [9,10,27,28]. The physics-inspired features are then used as inputs to AI/ ML algorithms for health

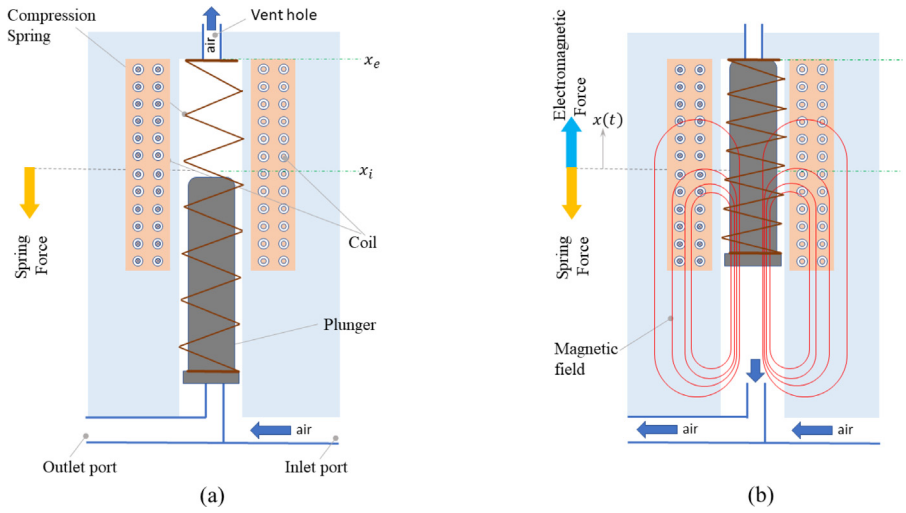

Fig. 1. The basic principle of a solenoid-operated valve (SOV). x_i and x_e respectively denote the rest position and the end-of-travel position of the plunger. (a) the SOV is de-energised, (b) the SOV is energised.

assessment, diagnostics and RUL predictions. Another possibility in the hybrid approach is by using a generic statistical feature as an input to the Bayesian filtering framework incorporating a degradation model for RUL estimations of SOVs [13,14].

Despite the fact that many efforts have been made in the development of CM and PHM technologies for DC-powered SOVs, notably, the CM and PHM technologies development for AC-powered SOVs reported in the literature is still very limited [8,24,25,28,29]. Thus, this gap leaves a room for further research and development on CM and PHM technologies for AC-powered SOVs.

1.2. Characteristics of an AC-powered SOV

It is worth of mentioning that AC-powered SOVs, which are the main focus of this study, have some important components comprising: plunger, return spring, casing and a special conductive ring coined "shading ring", see Fig. 2. The underlying physics for AC-powered SOVs is more complicated than that of DC-powered SOVs. Since AC current is approximately a sinusoidal waveform, the current signal has two zero-crossings per period.

Because the magnetic force generated by the solenoid is directly proportional to the electrical current that flows through the solenoid coil, the spring force will dominate the generated magnetic force at the two zero-crossing points for a short period of time. As a result, a vibration on the armature is generated, which produces a humming sound and can cause stress on SOV components. To avoid this problem, a special conductive ring coined "shading ring", usually made of copper, is placed near the coil around the armature, see Fig. 2(a). As stated in [30], the main purpose of a shading ring is to store magnetic energy and to release it with a 90 degree phase shift. While the magnetic field generated by the primary coil decreases to zero, the magnetic field generated by the shading ring reaches its peak, effectively filling the gap in the magnetic field amplitude during zero crossings, thus eliminating the vibrations. Most AC-powered SOVs that can be used with different coil voltages have a built-in shading ring.

Based on our previous accelerated life test (ALT) campaigns on 16 valves, two main failure modes were observed, namely (i) mechanical wear, and (ii) shading ring deterioration. Fig. 2 shows the cross-sections of a new and a damaged valve. As seen in the figure, the mechanical wear occurring on the plunger side and the plunger tube is due to the friction originating from the relative motion between the two. While, the impact wear occurs around

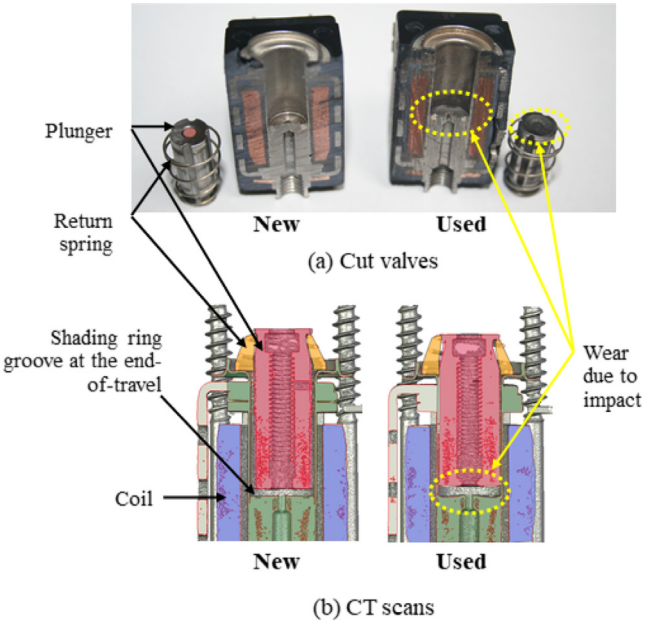

Fig. 2. (a) Cross section photos of two cut SOVs and (b) the CT scan images of both valves. New SOV (left) vs. degraded one (right) after an accelerated life test (ALT), reproduced from [29].

the top of the plunger and the end position of the plunger (end of travel) where the shading ring is located. This impact wear is due to the plunger vibration caused by the shading ring deterioration as explained above.

1.3. Failure modes, mechanisms and effects analysis (FMMEA)

As summarised in [3], in general, there are seven potential failure modes that can be observed on SOV parts, namely: (1) valve body, (2) seal, (3) core/plunger, (4) plunger spring, (5) coil housing, (6) plunger tube and (7) electrical coil. The early work conducted in 1987 at Oak Ridge National Laboratory (ORNL) showed that over 50% of SOV failures originated from four causes (i) worn or degraded parts, (ii) contamination by foreign materials, (iii) short circuit in the SOV coil, and (iv) open circuits in the SOV coil. The other failures were related to production and

(a) (b)

Fig. 3. (a) The photo of test setup for performing simultaneous ALTs on 48 AC-powered SOVs. (b) Close up view of individual valves and the mounted air flow sensors.

assembly defects, incorrect installation, loose/ misaligned parts, or the root cause that could not be determined.

Our previous results [29] of the first ALT campaign on 16 AC-powered SOVs revealed that the worn plunger, the worn plunger tube and the degraded shading ring coil are the main root causes of the AC-powered SOVs. This first ALT campaign was not equipped with temperature and air flow sensors that can serve as the ground truth for determining the end of useful life (EOL) of the SOVs in an objective manner. A year later, a follow-up ALT campaign equipped with the EOL ground truth measurement devices on 48 identical SOVs took place [24]. The results in this paper are based on the old and new datasets and confirm that most of the SOV failures have these root causes.

1.4. Objectives and main contributions

Since the development of CM and PHM technologies for AC-powered SOVs reported in the literature is still very limited as mentioned in Section 1.1, it is therefore necessary to research and develop further CM and PHM technologies for AC-powered SOVs to ensure that the technologies maturity level is achieved. The data-driven and hybrid based CM and PHM technologies for AC-powered SOVs have been proposed recently in the literature [24,25,28,29]. However, to the best of the authors' knowledge, the model-based CM and PHM technologies for AC-powered SOVs are not available yet in the literature. To this end, the main objective of this paper is develop model-based condition indicators (CIs) for AC-powered SOVs that can be later on used for diagnostics, condition monitoring and prognostics purposes.

First, we present the improvement of a first-principle model of AC-powered SOVs taking into account the degradation effects, namely (i) the shading ring degradation, and (ii) mechanical wear. Although first-principle models for DC-powered SOVs do exist in literature, see for example [22,31], these models do not take into account the shading ring force that represents the shading ring degradation level. In [32], a shading coil model is included in the model of AC-powered contactors, and a parametric study of some design parameters was investigated. The latter publication inspired our work to include shading ring force in the first-principle model of AC-powered SOVs. Thus, our work is complementary, and proposes a physical explanation behind the rationale of using a shading ring force based on a simple mathematical model. Numerical simulation results show that our model can explain quite well the experimental observations.

Second, we propose a method to extract three condition indicators (CIs) using the improved model and the measurement data. The CIs include (1) the shading ring force, (2) the kinetic Coulomb friction force, and (3) the area under the plunger displacement curve.

1.5. Paper organisation

The rest of this paper is structured as follows. Section 2 discusses experimental aspects. Section 3 presents the improvement of the physics-based model of AC-powered SOVs. Section 4 presents a method to extract condition indicators/features using the improved model and measurement data. Section 5 discusses the results obtained by applying the proposed methodology to the experimental data. Finally, Section 6 concludes with the main findings of this study and proposes future work.

2. Experiment

A solenoid endurance test setup was developed to perform simultaneous ALTs on 48 AC-powered SOVs, as shown in Fig. 3. The type of used valves are direct acting 3/2 way *normally closed* (Burkert Type 6014). The ALTs were performed at an ambient temperature of 25 °C by repeatedly switching the valves on and off at a rate of 1 Hz for a total duration of approximately 6 weeks. Each valve is powered by an input AC voltage of 110 V at 50 Hz and supplied with compressed air at 8 bar in the inlet port.

During the ALT campaign, both current and voltage signals were measured for each valve. Besides, the surface temperature and air flow rate of the SOV outlet just after the switch-on/off were also measured for each valve as a means to have the "ground truth data" for labelling the end of life of each valve in an objective way.

Figs. 4–6 show representative measurement signals (current, air flow outlet just after the switch-on/off) of a valve in healthy, faulty and failure case, respectively. We see in Fig. 4 that the current signal in the healthy case exhibits a distorted sinusoidal pattern with a dip in the first half period. Afterwards, multiple dips are observed on the current signal when the valve gets faulty as shown in Fig. 5. Eventually, the current signal becomes almost a pure sinusoidal signal when the valve has completely failed as shown in Fig. 6. Transient air flows are observed just after the valve is switched on/off for the healthy and faulty case. However, as expected, the air flow remains zero when the valve has completely failed, see Fig. 6.

The current signal through the solenoid was measured by a current transducer LEM CTSR 0.3-P at the sampling frequency of 50 kHz. The temperature and pressure of the air being supplied to each valve were measured by a thermocouple Pt100 and a pressure transducer GEMS 3100, respectively, at the sampling frequency of 1 Hz. The surface temperatures and the ambient temperatures around the valves were measured with thermocouples Pt100. The air flows of all the valves were measured by thermal mass flow sensors (IST AG FS7) at the sampling frequency

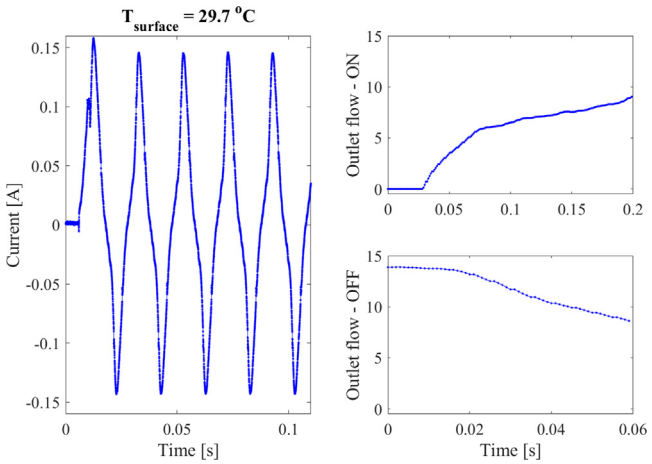

Fig. 4. Representative measurement signals of the AC current, outlet flows just after the switch-on and -off of a valve in a *healthy* case.

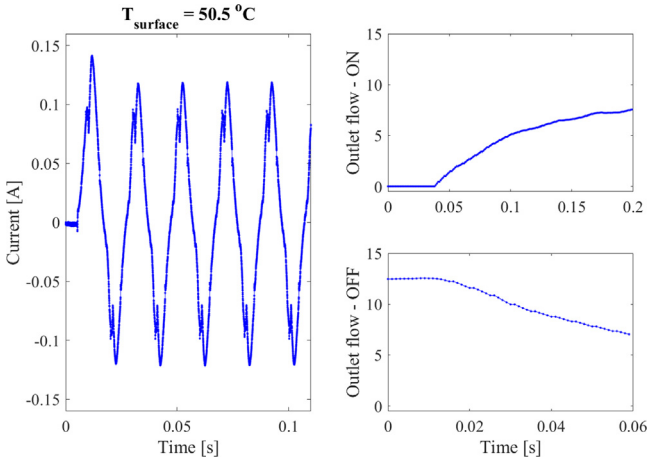

Fig. 5. Representative measurement signals of the AC current, outlet flows just after the switch-on and -off of a valve in a *faulty* case.

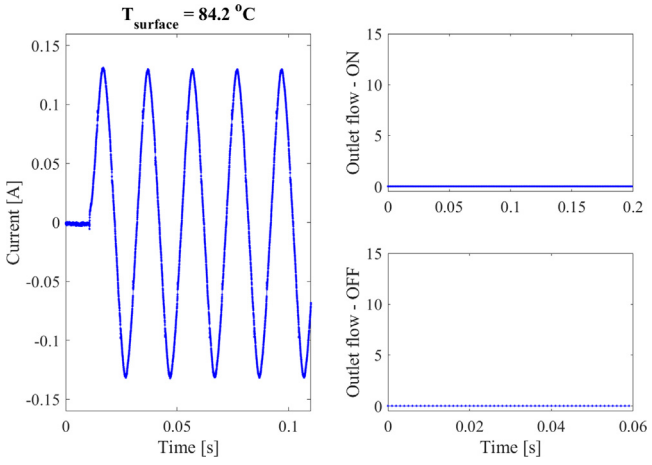

Fig. 6. Representative measurement signals of the AC current, outlet flows just after the switch-on and -off of a valve in a *failure* case.

of 1 kHz. All the sensory data were synchronously captured and recorded every minute for an acquisition duration of 0.5 s.

Fig. 7 shows the evolution of the area below the curve of the flow signals just after switch-on/off, $Q_{Out/ON}$ and $Q_{Out/OFF}$ (see the upper and middle graphs) and the surface temperature $T_{surface}$ (the lower graph) during the ALT of a valve. The leftmost vertical dashed line in the graphs represents the **onset of the shading ring degradation** which is visually determined by an expert on the current signals. Meanwhile, the rightmost vertical dashed line denotes the **end of useful life** of the valve which can be justified by the sudden drop of $Q_{Out/ON}$ and $Q_{Out/OFF}$ or the sudden increase of $T_{surface}$.

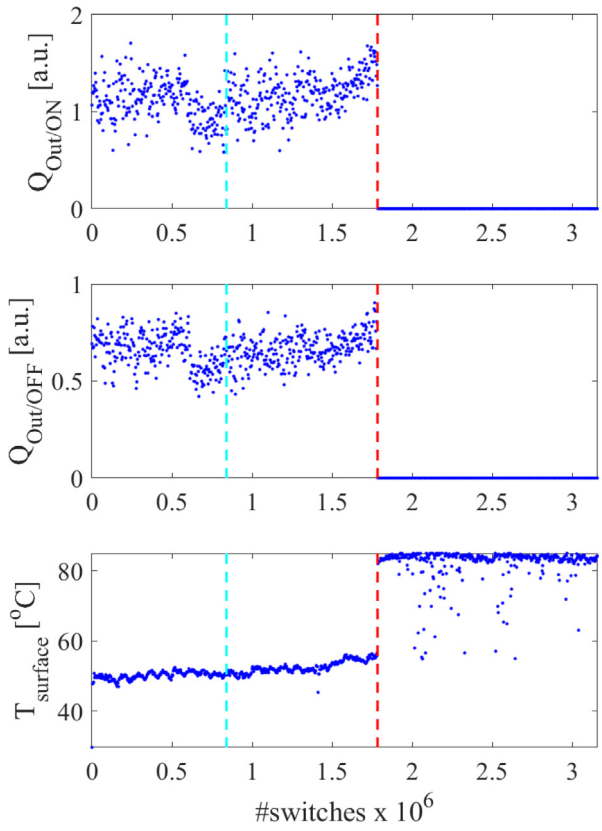

Fig. 7. Area below the curve of the flow signals just after switch On/Off and the surface temperature in function of the switch cycles.

3. Improvement of the first-principle model

In this section, we start by deriving a model based on first principles as well as its limitations and our proposals to overcome them.

At first, we do not include a shading ring in the model. In the electromagnetic circuit, see Fig. 8(b), Kirchhoff's voltage law leads to,

$$u = Ri + \frac{d\Psi}{dt} \tag{1}$$

where $\Psi(x,t) = N \cdot \phi(x,t)$, N is the number of coil windings and ϕ the magnetic flux. Rewriting Eq. (1) with the magnetic flux as the state of the system, this becomes,

$$\dot{\phi} = \frac{1}{N} \cdot \left(u - Ri\right) \tag{2}$$

The plunger of the valve is attached to the housing by a return spring. From a mechanical point of view, a balance of forces in the x direction leads to,

$$m \cdot \ddot{x} + c \cdot \dot{x} + k \cdot x = F_{pt} + F_{s \to p} \tag{3}$$

where m is the mass of the plunger, c is the viscous damping coefficient, k is the return spring constant, F_{pt} is the return spring

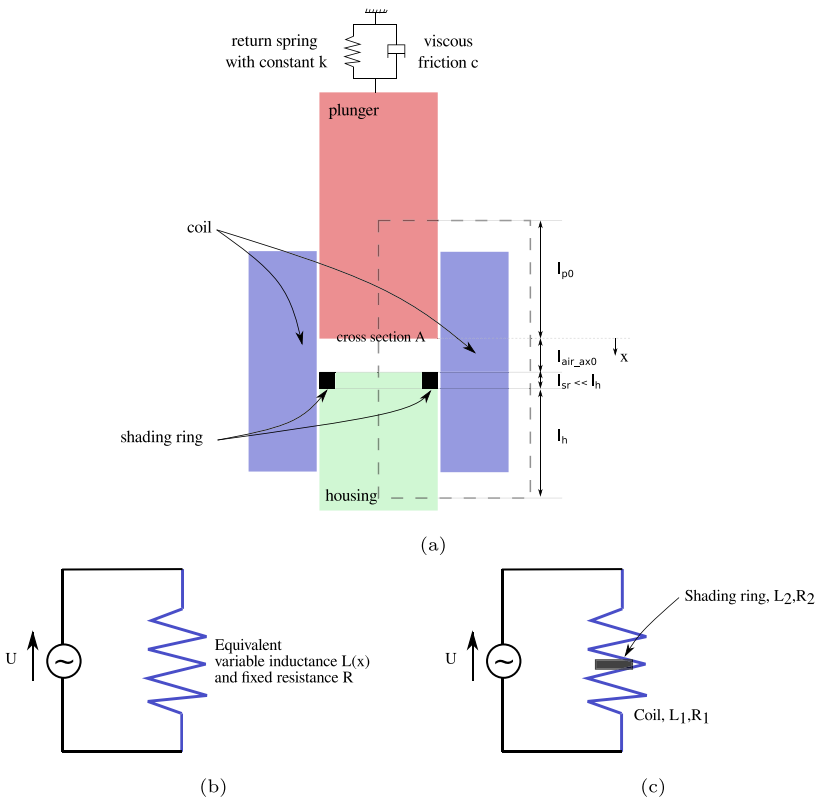

Fig. 8. Graphical representation of an AC-powered SOV: (a) main components comprising the main coil, the housing, the return spring and the shading ring. As the plunger moves, the inductance varies: in (b) an equivalent circuit without considering the shading ring. In (c) an equivalent circuit by isolating the coil and the shading ring: $\partial_x L_1 = 0$ is considered in the absence of plunger motion.

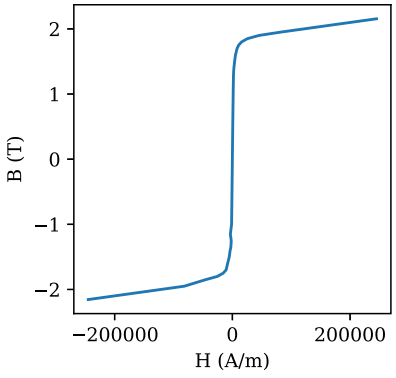

Fig. 9. B–H characteristic for the iron, no hysteresis has been considered. It is assumed both the plunger and the housing have the same B–H characteristic.

pretension (x_0) and $F_{s\to p}$ is the Lorentz force generated by the solenoid on the plunger. The coupled magnetic and mechanical equations can then be casted into the following system of equations,

$$\begin{cases} \dot{\phi} &= \frac{1}{N}\cdot\left(u - Ri\right) \\ \ddot{x} &= \frac{1}{m}\left(-c\cdot\dot{x} - k\cdot(x - x_0) + F_{s\to p}\right), \text{ with } 0 \le x \le l_{air_{ax}0} \end{cases} \tag{4}$$

The expression of the current can be obtained by applying Ampere's law on the contour (see Fig. 8(a)),

$$\oint_c H\cdot dl = \iint_{S_c} j\cdot dS \tag{5}$$

Since there are N windings traversing the cross section S_c, the right hand side is simply $N\cdot i$. The current can then be approximated by discrete portions on the chosen contour,

$$i = \frac{1}{N}\sum_n H_k\cdot l_k \tag{6}$$

where n sums over plunger, housing and axial air (air_{ax}). We neglect the radial components of the magnetic field intensity. By assuming the permeability of the air is the one of vacuum (μ_0),

$$H_{air_{ax}}\cdot l_{air_{ax}} = \frac{\phi}{\mu_0 A_{air_{ax}}}\cdot l_{air_{ax}}$$

where,

$$l_{air_{ax}} = l_{air_{ax}0} - x \tag{7}$$

Both the plunger and the housing are assumed to be made of iron with a nonlinear B–H characteristic without hysteresis, as illustrated in Fig. 9. The contribution to the sum in Eq. (6) from the plunger is,

$$H_p\cdot l_p = H_{iron}\left(\frac{\phi}{A_p}\right)\cdot l_p \tag{8}$$

where the plunger length that is covered by the contour l_p, can be expressed as a function of x and its initial length l_{p0},

$$l_p = l_{p0} + x \tag{9}$$

In a similar way, we arrive at the expression for the housing contribution,

$$H_h\cdot l_h = H_{iron}\left(\frac{\phi}{A_h}\right)\cdot l_h \tag{10}$$

where $l_h \approx l_{p0}$ and $A = A_p \approx A_h \approx A_{air_{ax}}$.

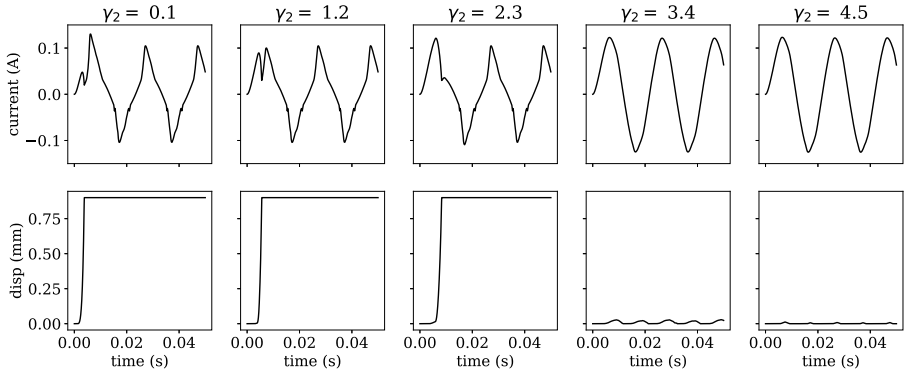

Fig. 10. Increasing the kinetic Coulomb friction force ($\gamma_2 \cdot F_{dc_0}$) in simulation leads to a longer time before the plunger hits the stopper (the first three plots). If the kinetic Coulomb friction force is too high, the plunger might not move anymore: leading to a fixed inductance, the circuit then behaves as an RL circuit: the current signatures become sinusoidal (two last plots).

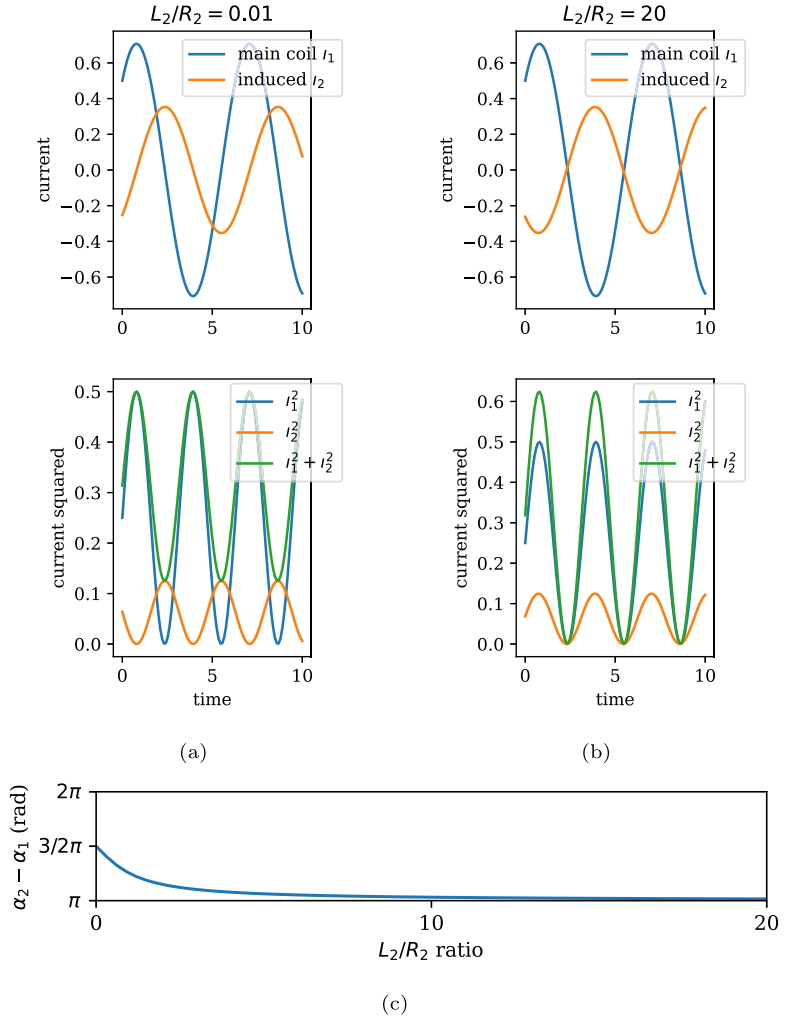

Fig. 11. Coil current (i_1) and induced current in the shading ring (SR) (i_2) illustrated for a couple of SR designs: (a) $L_2/R_2 = 0.01$ and in (b) $L_2/R_2 = 20$. Interestingly, if $L_2/R_2 \to 0$, then $\alpha_2 - \alpha_1 \to 3/2\pi$, see induced current phase w.r.t. coil current in (c). SRs are designed such that L_2/R_2 is small (b): the sum of the squares of the currents is never null, therefore a magnetic force will always be present. When this force is high enough, it will counteract the return spring force and maintain the contact inside the valve avoiding both leakage and the contact bounce phenomenon.

Finally, the Lorentz force generated by the solenoid on the plunger is obtained as follows:

$$F_{s\to p} = \int i \cdot dl \times B \tag{11}$$

Knowing that $Li = N\phi$ and $L = \mu_0 \cdot N^2 A/l$ (the detailed derivations of these relationships can be found in [22]), one obtains,

$$F_{s\to p} = \frac{\phi^2}{\mu_0 A} \tag{12}$$

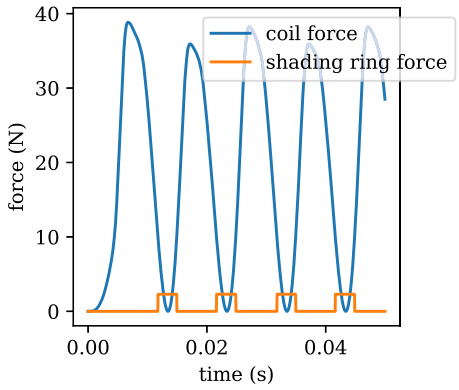

Fig. 12. Lorentz forces applied by the coil and the shading ring (F_{sh_0}) on the plunger. The latter is modelled as a rectangular periodic function with the same period as the coil current (and therefore force) but translated out of phase as explained in Fig. 11.

Using the previous equations, Eq. (4) can then be expressed as a function of ϕ, x and some parameters,

$$\begin{cases} \dot{\phi} &= \frac{1}{N}\cdot u - \frac{R}{N^2}\cdot\left((l_{air_{ax}0}-x)\cdot\frac{\phi}{\mu_0 A}+H_{iron}\left(\frac{\phi}{A}\right)\cdot(2\cdot lp_0+x)\right) \\ \ddot{x} &= \frac{1}{m}\left(-c\cdot\dot{x}-k\cdot(x-x_0)+\frac{\phi^2}{\mu_0 A}\right),\ \text{with } 0\le x\le l_{air_{ax}0} \end{cases} \tag{13}$$

Such a system of ordinary differential equations (ODEs) can be casted as a nonlinear state space system and solved using any solver. In our case, it was chosen to be implemented in Matlab/Simulink and solved using a fourth order Runge–Kutta solver.

The endurance test campaign has shown that after some hundreds of thousands of cycles, AC valves can start to leak and exhibit undesired vibrations which are due to the contact bouncing phenomenon [32]. To our knowledge, no valve physical models such as the one derived above and found in the literature contain unstationary physically meaningful parameters that could explain the change in current signatures during their lifetimes [32,33]. To address these issues, we introduce two additional time-dependent forces to the classical model developed earlier, on the time scale of the life of AC-powered SOVs,

$$\begin{cases} \dot{\phi} &= \frac{1}{N}\cdot u - \frac{R}{N^2}\cdot\left((l_{air_{ax}0}-x)\cdot\frac{\phi}{\mu_0 A}+H_{iron}\left(\frac{\phi}{A}\right)\cdot(2\cdot lp_0+x)\right) \\ \ddot{x} &= \frac{1}{m}\left(-c\cdot\dot{x}-k\cdot(x-x_0)+\frac{\phi^2}{\mu_0 A}+\gamma_1\cdot F_{sh_0}+\gamma_2\cdot F_{dc_0}\right) \\ & \text{with } 0\le x\le l_{air_{ax}0} \end{cases} \tag{14}$$

These additional forces are the kinetic Coulomb friction force (F_{dc_0}) and the shading ring force (F_{sh_0}). An explanation of the physical laws behind the contact bouncing phenomenon and the shading ring forces is lacking in the existing literature. Therefore, the ambition of the next paragraphs is also to give a clear physical understanding of the role of shading rings in AC contactors and valves.

3.1. Coulomb friction forces

The inspection of multiple computed tomographies, see an example in Fig. 2(b), shows wear due to the impact of the plunger on the stopper, which means that some material and debris detach from both plunger and housing during their lifetime. A manual inspection of the valves reveals that friction has appeared between the beginning and the end of life between plunger and housing. While this does not necessarily motivate the type of friction that should be introduced in the model, simulation results presented in Fig. 10 show that the increase of a kinetic Coulomb friction force moves the first 'bump' in the current signatures to the right: this corresponds to an increasing 'time to hit' of the plunger on the stopper, when the valve degrades during its lifetime. The shift in time of this 'bump' has been observed in the experimental data giving confidence in the non-stationary driver of the observations in that respect: the kinetic Coulomb friction force introduced in the model is,

$$\begin{cases} \text{if} & |\dot{x}| > 10^{-4}, F_{dc_0} = f\cdot\text{sign}(\dot{x}) \\ \text{else,} & F_{dc_0} = 0 \end{cases}$$

3.2. Phase of the magnetic force developed by shading rings

While a kinetic Coulomb friction force can explain the lag in the plunger hit on the stopper, this subsection explains the contact bounce phenomenon observed during the lifetime of the valves. To this end, we introduce a shading ring force in the classical model.

Note that, without considering the shading ring in Fig. 8(b), the system can be considered as an RL circuit, governed by the equation,

$$u = L_1\frac{di_1}{dt} + Ri_1 \tag{15}$$

This is an AC system, so we describe the input voltage as,

$$u(t) = U_m\cdot\cos(\omega t) \tag{16}$$

where $\omega = 2\pi\cdot 50$ rad and $U_m = 110$ V. An analytical solution of Eq. (15) is known to be,

$$i_1(t) = I_{m_1}\cdot\cos(\omega t+\alpha_1) \tag{17}$$

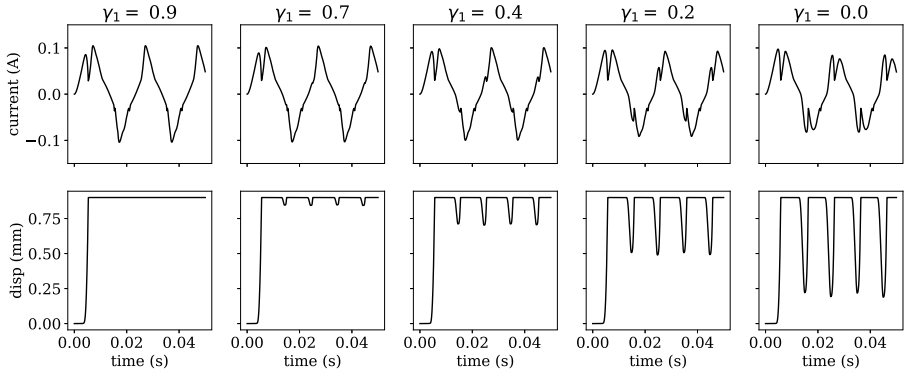

Fig. 13. Simulated effect of decreasing the shading ring nominal force: $F_{sh} = \gamma_1\cdot F_{sh_0}$. On the very left, the single bump in the current corresponds to the first hit of the plunger on its stopper (see plunger displacement on bottom plot). As the nominal shading ring force decreases, additional bumps emerge on the current signatures: this is the contact bounce phenomenon observed experimentally.

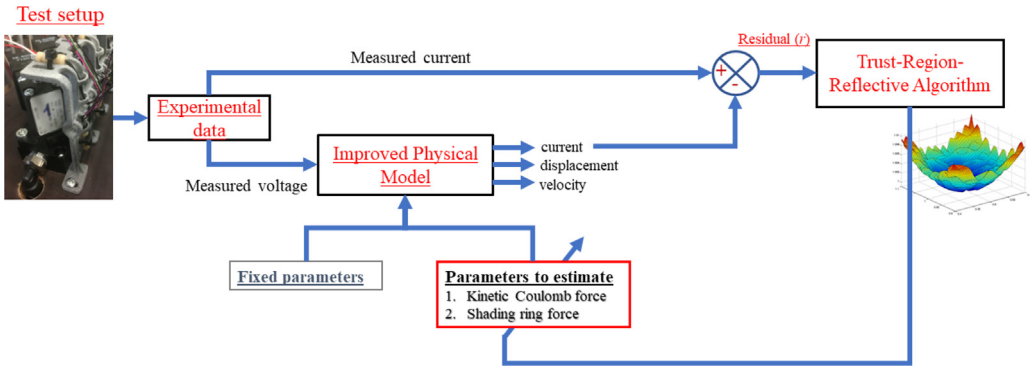

Fig. 14. Block diagram describing the identification procedure.

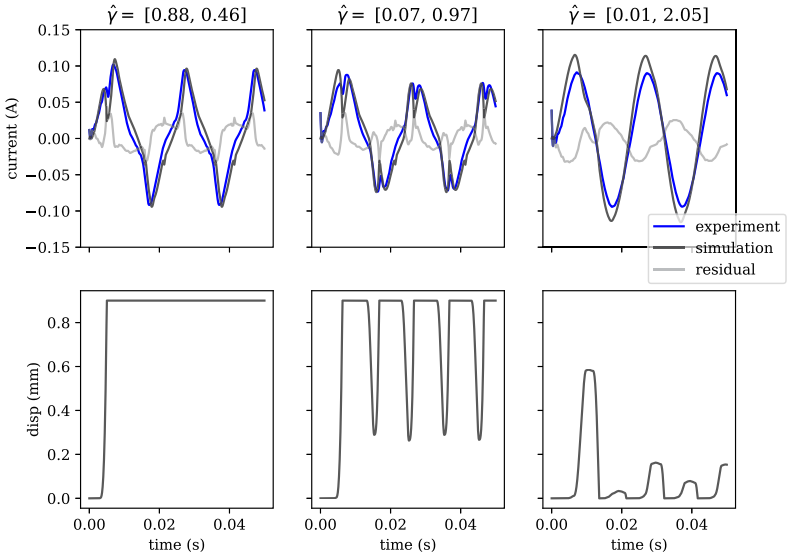

Fig. 15. Estimation of two CIs $\hat{\gamma}$ (shading ring and kinetic Coulomb friction forces) from the proposed model leads to a close match with the experimental current signatures. The three main stages during the lifetime of AC valves are identified. On the bottom plots, the physical model gives insights on the position of the plunger which is quite insightful and very hard to measure. The residual error is not null revealing our model does not capture all the dynamics of the system, it is however sufficient to explain the health condition of all the tested valves.

where the current magnitude is,

$$I_{m_1} = \frac{U_m}{\sqrt{R_1^2 + \omega^2 L_1^2}} \tag{18}$$

and the current phase α_1 with respect to the input voltage,

$$\alpha_1 = -\arctan\left(\frac{\omega L_1}{R_1}\right) \tag{19}$$

The magnetic force that attracts the plunger inside the coil is proportional to $i_1(t)^2$ and will therefore be null at every time t_{null},

$$t_{null} = \frac{\alpha_1}{\omega} + 2p\pi \tag{20}$$

where p is an integer. Since the physical system contains a return spring, without a shading ring the valve will try to return to its initial position whenever $t = t_{null}$. By introducing a shading ring at the centre of the coil, see Fig. 8(b), an electromotive force e will appear in the shading ring, according to Faraday's law of induction,

$$e = -\frac{d\Phi}{dt} \tag{21}$$

where $\Phi(t) = L_1 i_1(t)$. Therefore, the current induced inside the shading ring will satisfy the following equation,

$$e = L_2 \frac{di_2}{dt} + R_2 i \tag{22}$$

To find an analytical solution to this equation, we introduce a couple of notations using complex numbers. First for the current in the coil,

$$\underline{i}_1 = I_{m_1} \cdot e^{j\omega t + \alpha_1} = \underline{I_{m_1}} \cdot e^{j\omega t} \tag{23}$$

and second for the induced current inside the shading ring,

$$\underline{i}_2 = I_{m_2} \cdot e^{j\omega t + \alpha_2} = \underline{I_{m_2}} \cdot e^{j\omega t} \tag{24}$$

Eq. (22) can be simply reformulated,

$$-L_1 j\omega \underline{I_{m_1}} = \underline{I_{m_2}}(L_2 j\omega + R_2) \tag{25}$$

Therefore,

$$\underline{I_{m_2}} = \frac{-L_1 j\omega \underline{I_{m_1}}}{L_2 j\omega + R_2} \tag{26}$$

Finally, the amplitude of the induced current will be,

$$I_{m_2} = \frac{U_m L_1 \omega}{\sqrt{(R_1^2 + \omega^2 L_1^2)(R_2^2 + \omega^2 L_2^2)}} \tag{27}$$

and its phase α_2,

$$\alpha_2 - \alpha_1 = \arg(\underline{I_{m_2}}) - \alpha_1 = \frac{3\pi}{2} - \arctan\left(\frac{\omega L_2}{R_2}\right) \tag{28}$$

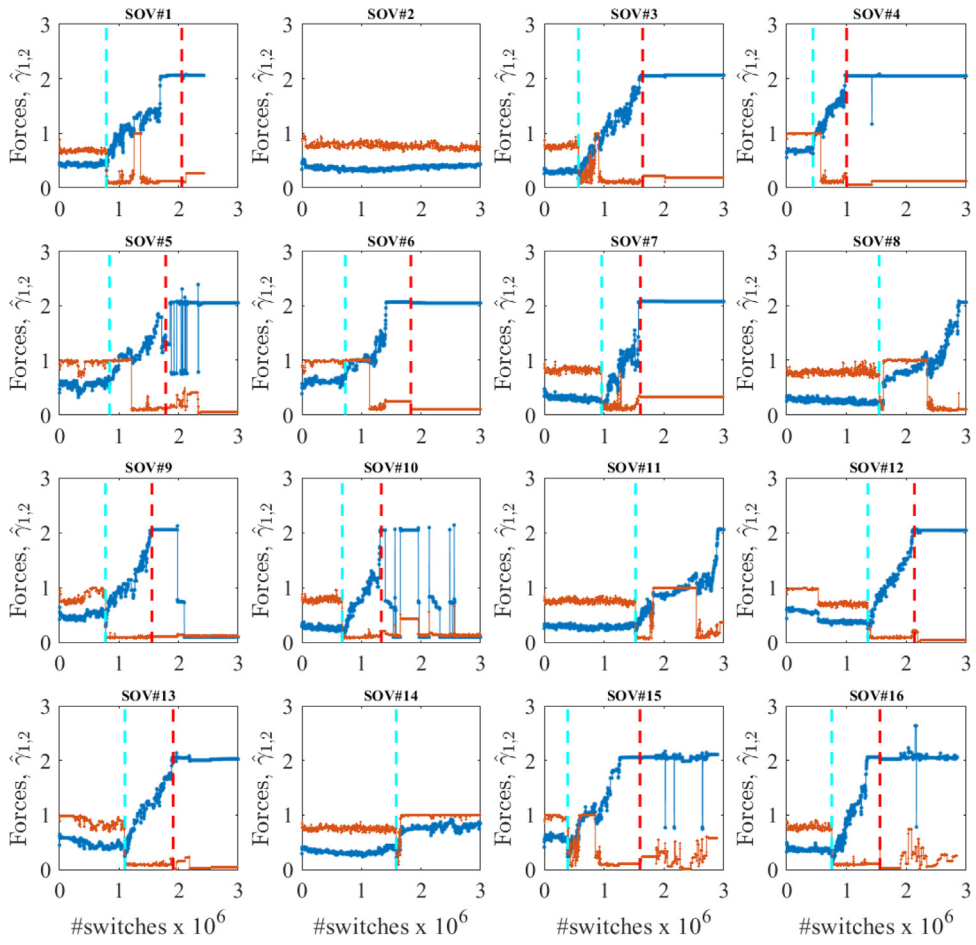

Fig. 16. Evolution of the identified Coulomb friction force (blue curves) and shading ring force (red curves) of SOV#1–SOV#16 during their lifetimes. (For interpretation of the references to colour in this figure legend, the reader is referred to the web version of this article.)

These expressions for the magnitudes and the phases of the currents allow to better understand the role of shading rings in AC valves, which is illustrated in Fig. 11.[1]

As can be seen in Fig. 11, an optimal shading ring design is the one where L_2/R_2 is small leading to a Lorentz force out of phase with the one of the main coil. Therefore, we choose to model the shading force (F_{sh_0}) as a rectangular periodic function with the same period as the coil current (and therefore force) but translated out of phase, see Fig. 12. For this surrogate model of the shading ring force, we assume that the amplitude of the rectangle varies depending on the health condition of the AC valve, which is a parameter that will be identified (γ_1). The choice to use this surrogate model rather than a more detailed model of the force is justified by the results obtained when comparing simulations with experimental results (in the next section): these show that our assumption on the necessary model complexity is sufficient.

Fig. 13 shows the effect of the shading ring degradation (indicated by the shading ring force reduction) on the current signal. As seen in the figure, the shading ring degradation causes additional bumps on the current signal that leads to the plunger vibrating as discussed in Section 1.2.

4. Method for extracting condition indicators (CIs) from the model and the experimental data

The previous section motivated the introduction of two non-stationary forces, at the time scale of the lifetime of AC valves into a state of the art AC valve physical model. These forces, parameterised by γ_1 and γ_2, characterise the amounts of the shading ring and kinetic Coulomb friction forces respectively during the lifetime of the valves. As shown in the previous section, the variation of these two parameters (see Appendix) in simulation explain the observed variations in the experimental current signatures during the valves' lifetimes. This section explains how to identify those forces. Notably, the results confirm the validity of our assumption that these two forces are the main drivers of the health condition of the valves.

To estimate those forces, which are our condition indicators (CIs), the residual error (r) between experimental current measurements and simulated currents is introduced:

$$r(\gamma) = \frac{1}{n}\|i_{exp} - i_{sim}(\gamma)\|^2 \tag{29}$$

where i_{exp} is the experimentally measured current during our endurance test campaign and $\gamma = [\gamma_1, \gamma_2]^T$ is a vector representing possible solutions for the shading ring and kinetic Coulomb friction forces. Since the simulated current $i_{sim}(\gamma)$ is a nonlinear function, the problem is formulated as a nonlinear least-squares problem:

$$\hat{\gamma} = \text{argmin}_{\gamma,\gamma_0}\left(\frac{1}{n}\|i_{exp} - i_{sim}(\gamma)\|^2\right) \tag{30}$$

This problem could be solved numerically using the trust-region-reflective algorithm [34] using the Matlab Optimisation Toolbox. The identification procedure is schematically shown in Fig. 14.

[1] For the sake of simplicity and without loss of generality, the following values where used $U_m = \omega = R_1 = L_1 = 1$.

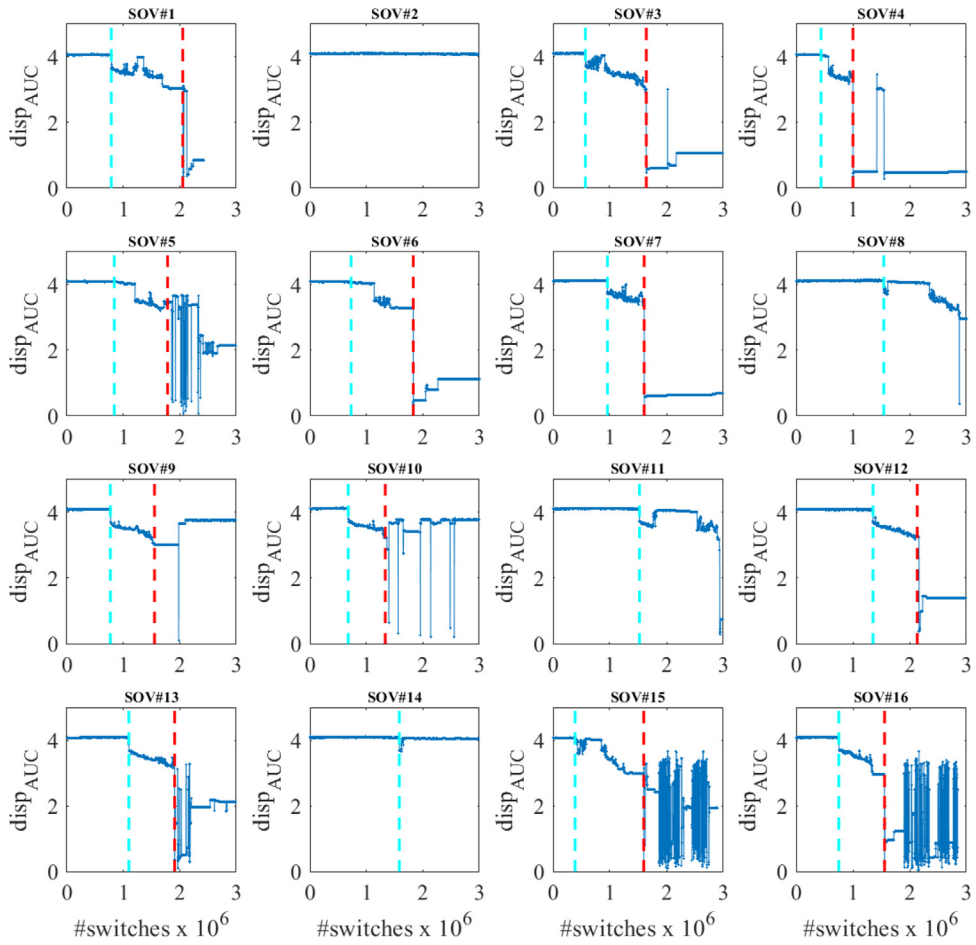

Fig. 17. Evolution of the area below the displacement curve of SOV#1–SOV#16 during their lifetimes.

In order to help the optimiser to switch between different degradation stages, the initial guess γ_0 is chosen among the smallest of the following residuals,

$$\begin{cases} r(\gamma_h) & \text{where } \gamma_h = [1, 1]^T \text{ simulates a healthy valve} \\ r(\gamma_s) & \text{where } \gamma_s = [0.01, 5]^T \text{ an unhealthy valve with a stuck plunger} \\ r(\hat{\gamma}_{t-1}) & \text{where } \hat{\gamma}_{t-1} \text{ is the estimation in previous time step} \end{cases}$$

Fig. 15 illustrates how some stages of health can be simulated and identified properly by the proposed approach. A single identification can be performed on a low-end CPU such as an Intel Core i7-6600U CPU (@ 2.60 GHz ×4) in less than 30 s.

Notably, the proposed methodology also allows to perform a virtual sensing on the displacement of the plunger by using the improved model and the measured current and voltage signals as described in Fig. 14. Some representative results after applying the identification procedure are shown in Fig. 15. Since the virtually measured plunger displacement also conveys information about the health condition of an SOV, a third CI can therefore be extracted. We define this new CI as the area below the curve of the plunger displacement signal $\mathbf{disp_{AUC}}$:

$$\mathbf{disp_{AUC}} = \int_{t_i}^{t_f} x dt, \tag{31}$$

with x denoting the plunger displacement signal, $t_i = 0$ denoting the initial acquisition time and t_f denoting the final acquisition time.

As the proposed methodology employs an improved first-principle model, it offers two main advantages. The first advantage is that the three condition indicators (CIs) extracted with the proposed methodology have physical meaning, so they can be easily interpreted and the links with the two main failure modes, namely mechanical wear and shading ring degradation, can be made. The second advantage is that first principle models typically have less free parameters than their data-driven counterparts and therefore the proposed methodology will not require lots of run-to-failure data to identify the parameters (i.e. CIs), as these data are typically not available in practice.

5. Results and discussion

The experimental data obtained in the test campaign described in Section 2 have been analysed offline using the developed methodology discussed in Section 4. As a result, three condition indicators (CIs), namely (1) the shading ring force and (2) the kinetic Coulomb friction force and (3) the area below the plunger displacement curve, were calculated for all the 48 SOVs. Figs. 16–21 show the evolution of the three CIs for all the valves. Note that the leftmost and rightmost vertical dashed-lines in each graph represent the ground truths that indicate the moments of the onset of shading ring degradation and the end-of useful life of each SOV, respectively. The leftmost vertical dashed-lines are determined by an industrial expert through a visual inspection on the current signal measurements of all the valves, while the rightmost vertical dashed-lines are inferred from the valve surface temperature and outlet flow measurements.

As shown by the experimental data, the surface temperature increases, and the outlet flow rate becomes zeros when an SOV has reached the end of useful life (EOL), see Fig. 7. These phenomena are explained as follow. When the plunger and the plunger

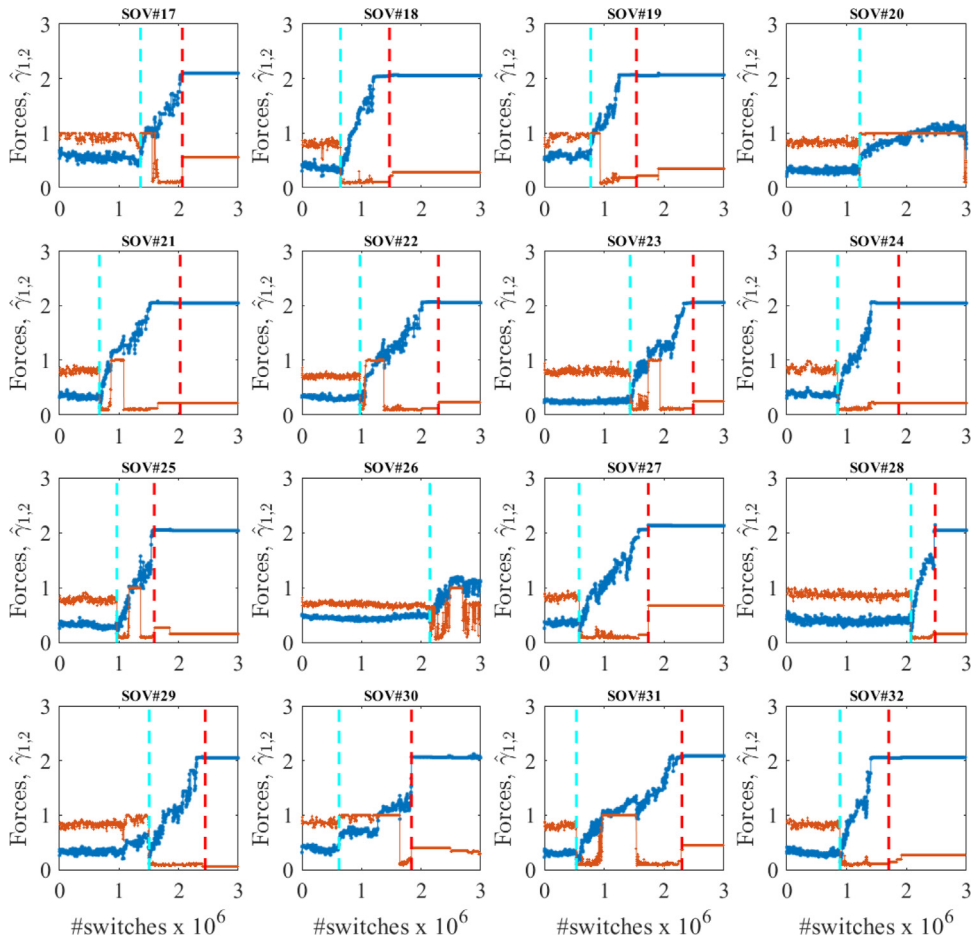

Fig. 18. Evolution of the identified Coulomb friction force (blue curves) and shading ring force (red curves) of SOV#17–SOV#32 during their lifetimes. (For interpretation of the references to colour in this figure legend, the reader is referred to the web version of this article.)

tube wear out (see Fig. 2), the friction force between the plunger and the plunger tube increases as experimentally validated by the improved first-principle model and the proposed methodology presented in Section 3. The evolution of the predicted friction force for all the valves is shown in Figs. 16, 18 and 20. As a result of the increased friction force, more heat is dissipated to the valve which eventually will increase the surface temperature. Furthermore, when the wear progresses further the friction force becomes too high, thus hampering the plunger motion which is in an agreement with the simulation results in Section 3.1. At this stage, the valve has reached the EOL since it is no longer able to flow out the air at the outlet port (i.e. the outlet flow rate is zero).

For the valves that have degraded or reached the failure state, the graphs show systematic changes of the three CIs during the valve lifetimes. On the other hand, for the valves that have not degraded or partially degraded (e.g. SOV#2, SOV#14, SOV#20, …), the three CIs do not show systematic changes, as expected.

In general, one can see that the kinetic Coulomb friction force γ_2 increases during the valve's lifetime. On the contrary, the shading ring force γ_1 tends to decrease as the degradation progresses. Furthermore, one can clearly see that the area below the plunger displacement curve disp_{AUC} tends to decrease during the valve's lifetime. The latter can be explained due to the fact that the friction force increases because of wear (see Fig. 2).

It is worth of mentioning that the kinetic Coulomb friction force γ_2 exhibits the most gradual (monotonic) change if compared with the other 2 CIs, namely (i) the shading ring force γ_1 and (ii) the area below the plunger displacement curve disp_{AUC}. This suggests that the kinetic Coulomb friction force γ_2 is a potential candidate to be used for remaining useful life (RUL) prediction. Nonetheless, the other 2 CIs are still useful for diagnosis purposes that could help the maintenance engineer to better understand and justify the status of a valve, e.g. to check whether the shading ring of a valve has degraded.

Notably, the estimation of the three CIs using the proposed methodology is rather unstable after the valves have reached or passed the end of useful life (indicated by the rightmost vertical dashed lines). Nevertheless, this is not really a problem for condition monitoring purposes, because the CIs are only relevant before the end of useful life.

Although all the 48 SOVs are identical and were under the same test conditions, the graphs show that each valve degrades differently. Two out of 48 valves (4% of the total population) did not experience a shading ring degradation nor wear. Meanwhile, twelve out of 48 valves (25% of the total population) did not reach the end of useful life. Furthermore, the histograms of the onset of shading ring degradation and the end of useful life, shown in Fig. 22, demonstrate the large variation of the degradation process. This large variation confirms the need of a CBM/PdM strategy supported by condition monitoring technologies for each individual valve for a more accurate health estimation and prediction, in order to schedule the maintenance action in a more optimal way.

6. Conclusions and outlook

We have presented an extended physical model to explain the health condition and occurring failure modes of AC-powered

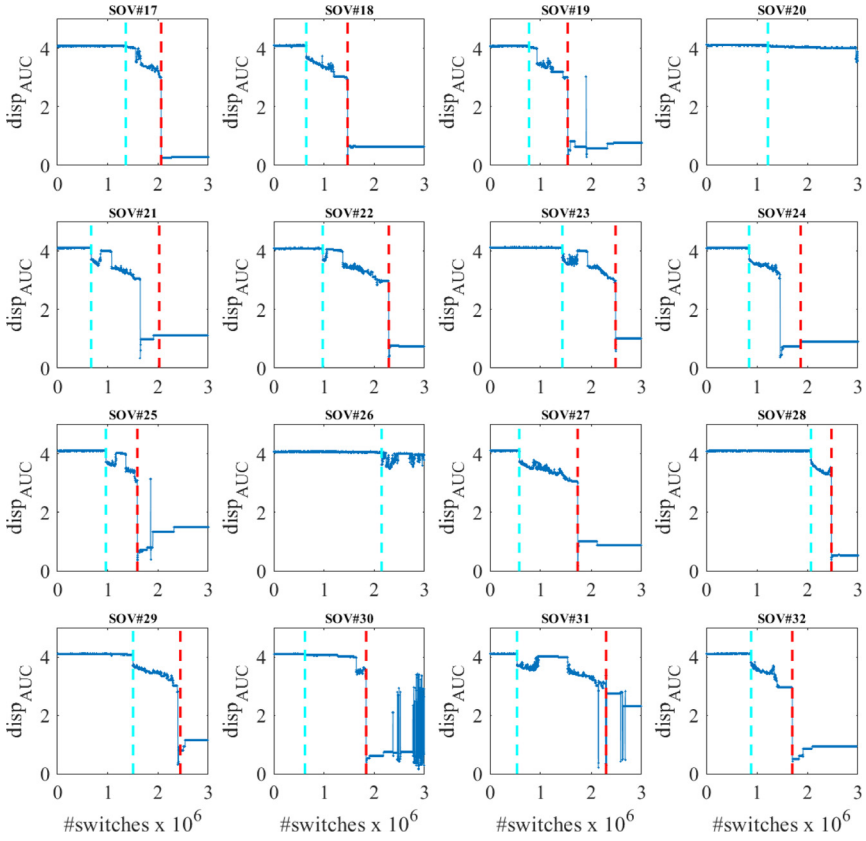

Fig. 19. Evolution of the area below the displacement curve of SOV#17–SOV#32 during their lifetimes.

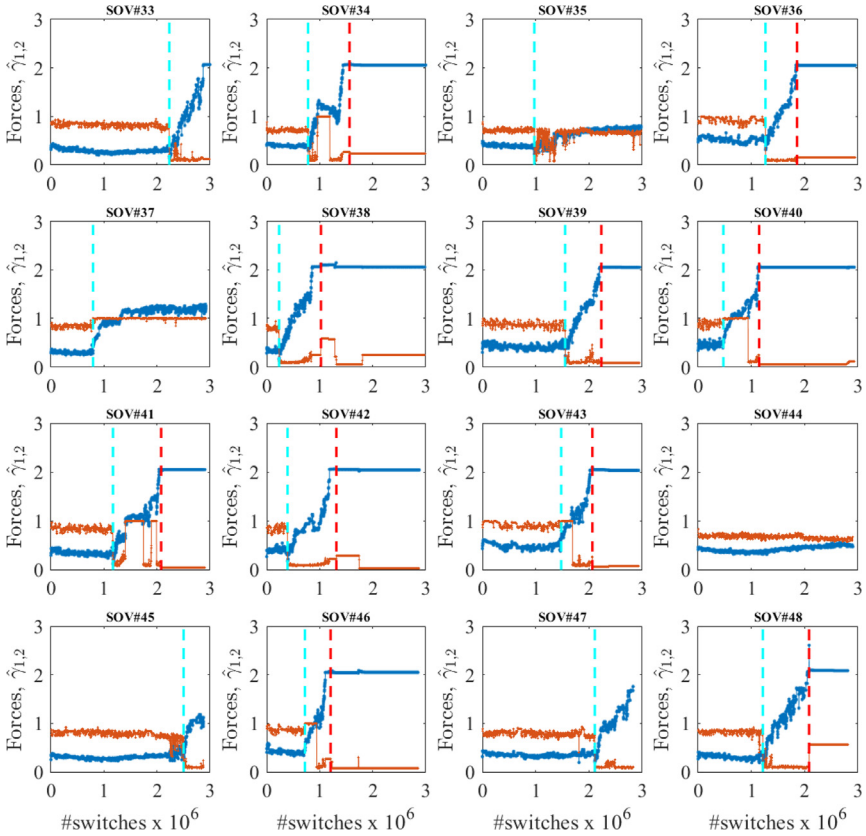

Fig. 20. Evolution of the identified Coulomb friction force (blue curves) and shading ring force (red curves) of SOV#33–SOV#48 during their lifetimes. (For interpretation of the references to colour in this figure legend, the reader is referred to the web version of this article.)

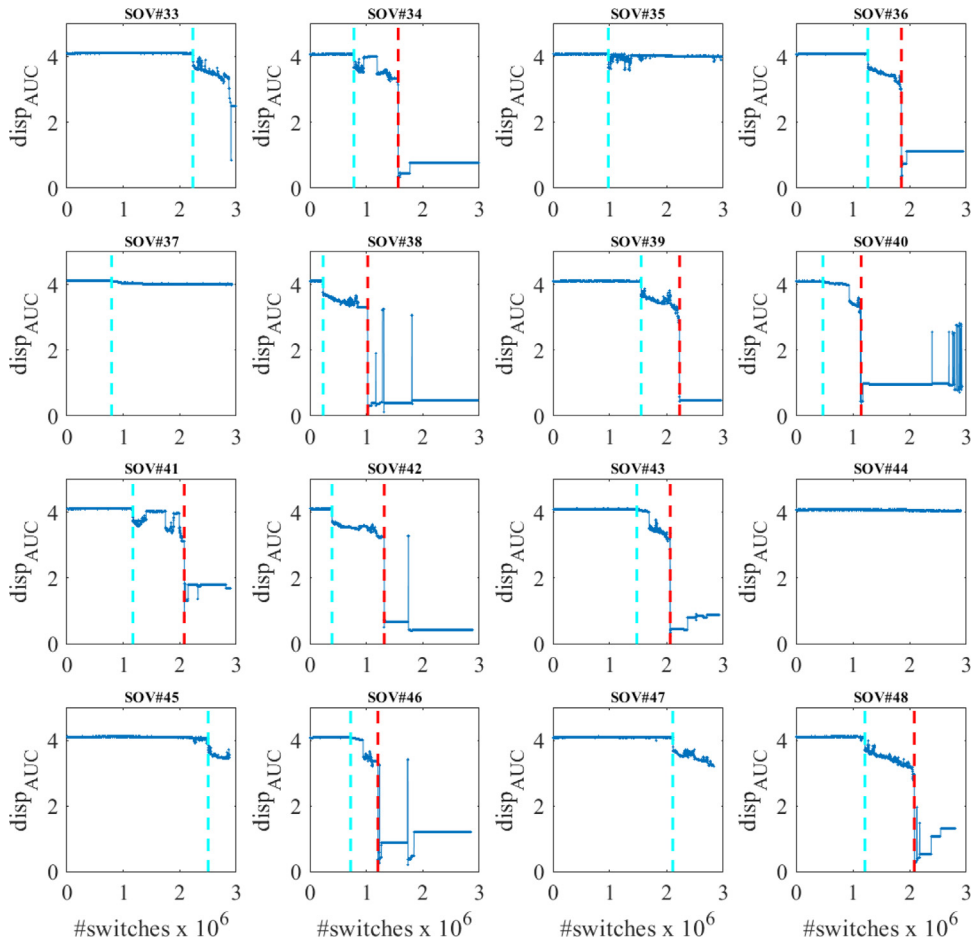

Fig. 21. Evolution of the area below the displacement curve of SOV#33–SOV#48 during their lifetimes.

SOVs during their lifetimes. This was experimentally validated using the datasets obtained from an ALT campaign on 48 AC-powered SOVs. The experimental results are in agreement with the simulation results generated by the improved model, confirming that the extended model is an improvement that can be used for health assessment. From this model, we devised a method to extract three condition indicators (CIs) from live current measurements, namely (1) the shading ring force, (2) the kinetic Coulomb friction force and (3) the area below the plunger displacement curve. We have analysed the value of these CIs for remaining life prediction: the kinetic Coulomb friction force shows gradual changes (monotonically increasing trends) over the lifetime of the valve making it suitable for prognostics purposes. On the contrary, the other two condition indicators exhibit rather abrupt changes when the shading ring starts to degrade, hence they are suitable for diagnostics purposes (i.e. determination of the failure mode types).

This study has demonstrated a large variance in the degradation of the valves. Therefore, for scheduling the maintenance action in a more optimal way for each individual valve, there is a high need of condition monitoring and prognostics and health management technologies for a more accurate SOV health estimation and prediction. The improved model and CIs presented make this possible.

Future work will be consisting of further research and development of diagnostics tool for the different failure modes, and prediction methods for the remaining useful life using the proposed CIs. Particular attention will be paid towards adequately taking into account prediction uncertainty in a condition-based maintenance strategy.

Table 1
List of model parameters.

Symbol	Description	Value [Unit]
N	Number of main coil winding	7000 [–]
$V(t)$	Input AC voltage	110 [V]
R	Coil resistance	1145 [Ω]
m	Mass of the plunger	4 [g]
c	Viscous damping coefficient	10 [Ns/m]
k	Return spring stiffness	200 [N/m]
F_{pt}	Return spring pretension force	2 [N]
μ_0	Air permeability	$4\pi\,10^{-7}$ [H/m]
$l_{\text{air}_{ax,0}}$	Maximal axial airgap	0.9 [mm]
l_h	Housing length	14.3 [mm]

Declaration of competing interest

The authors declare that they have no known competing financial interests or personal relationships that could have appeared to influence the work reported in this paper.

Acknowledgements

This research was performed in the framework of the industrial MODA ICON project (The contract number: HBC.2017.0392), funded by Flanders Make, Belgium, the strategic research centre for the manufacturing industry, and VLAIO, Belgium.

Appendix

See Table 1.

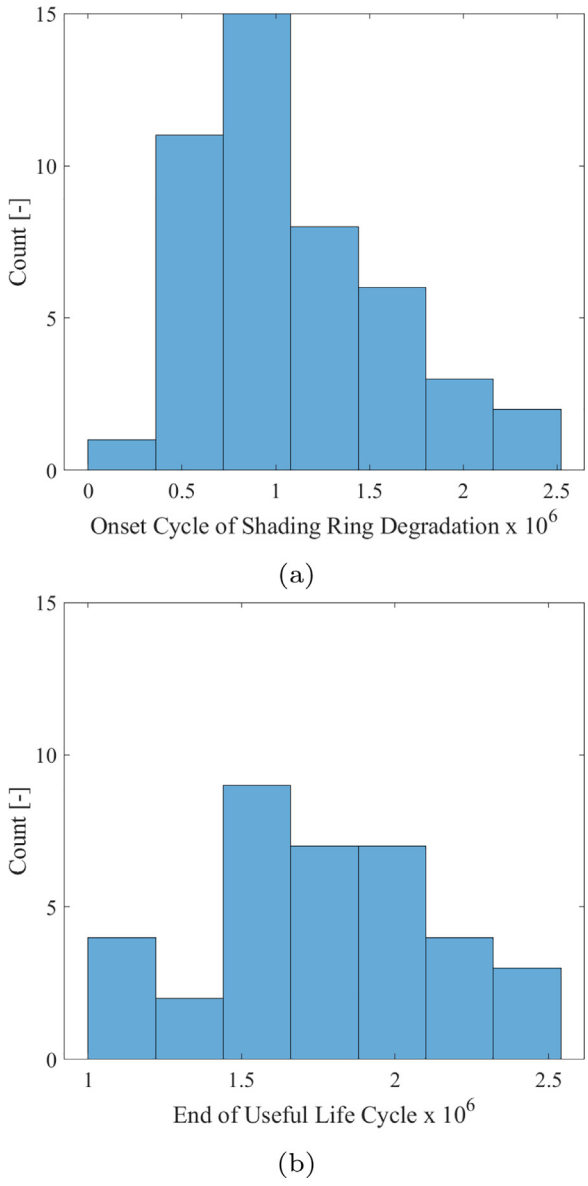

Fig. 22. The histogram of (a) the onset cycle of shading ring degradation, (b) the end of useful life, of all the valves.

References

[1] Zonta Tiago, da Costa Cristiano André, da Rosa Righi Rodrigo, de Lima Miromar José, da Trindade Eduardo Silveira, Li Guann Pyng. Predictive maintenance in the industry 4.0: A systematic literature review. Comput Ind Eng 2020;150:106889. http://dx.doi.org/10.1016/j.cie.2020.106889, URL https://www.sciencedirect.com/science/article/pii/S0360835220305787.

[2] Lei Yaguo, Li Naipeng, Guo Liang, Li Ningbo, Yan Tao, Lin Jing. Machinery health prognostics: A systematic review from data acquisition to RUL prediction. Mech Syst Signal Process 2018;104:799–834. http://dx.doi.org/10.1016/j.ymssp.2017.11.016, URL https://www.sciencedirect.com/science/article/pii/S0888327017305988.

[3] Jameson NJ, Azarian MH, Pecht M. Fault diagnostic opportunities for solenoid operated valves using physics-of-failure analysis. In: 2014 international conference on prognostics and health management. 2014, p. 1–6.

[4] Kryter Robert C. Nonintrusive methods for monitoring the operational readiness of solenoid-operated valves. Nucl Eng Des 1990;118(3):409–17.

[5] URL https://safety4sea.com/incinerator-fire-due-to-dirty-solenoid-valve/.

[6] Bly M. Deepwater horizon accident investigation report. first ed.. DIANE Publishing; 2011.

[7] Bacanskas VP, Roberts GC, Toman GJ. Aging and service wear of solenoid-operated valves used in safety systems of nuclear power plants: Volume 1, operating experience and failure identification. Technical report, (NUREG/CR-4819-Vol.1; ORNL/Sub-83-28915/4/V1). 1987.

[8] Kryter RC. Aging and service wear of solenoid-operated valves used in safety systems of nuclear power plants. Volume 2, evaluation of monitoring methods. Technical report, (NUREG/CR-4819-Vol.2; ORNL/TM-12038-Vol.2). 1992.

[9] Perotti Jose M, Lucena Angel, Ihlefeld Curtis, Burns Bradley, Bassignani Mario. Current signature sensor. 2005, Google Patents, US Patent 6, 917, 203 B1 URL https://patents.google.com/patent/US6917203B1/en?oq=US+6%2c917%2c203+B1.

[10] Perotti JM. KEA-71 smart current signature sensor (SCSS). NASA tech report no. 20110000497, 2010.

[11] Daigle Matthew J, Goebel Kai. A model-based prognostics approach applied to pneumatic valves. Int J Prognost Health Manag 2011;2(2):84–99.

[12] Tang X, Peng J, Chen B, Jiang F, Yang Y, Zhang R, et al. A parameter adaptive data-driven approach for remaining useful life prediction of solenoid valves. In: 2019 IEEE international conference on prognostics and health management. 2019, p. 1–6.

[13] Tang Xilang, Xiao Mingqing, Liang Yajun, Hu Bin, Zhang Lei. Application of particle filter technique to online prognostics for solenoid valve. J Intell Fuzzy Systems 2018;35:1–10.

[14] Tang Xilang, Xiao Mingqing, Hu Bin. Application of Kalman filter to model-based prognostics for solenoid valve. Soft Comput 2019;1–13.

[15] Peng Jun, Tang Xuanheng, Chen Bin, Jiang Fu, Yang Yingze, Zhang Rui, et al. Failure type prediction using physical indices and data features for solenoid valve. Appl Sci 2020;10(4).

[16] Jo Soo-Ho, Seo Boseong, Oh Hyunseok, Youn Byeng D, Lee Dongki. Model-based fault detection method for coil burnout in solenoid valves subjected to dynamic thermal loading. IEEE Access 2020;8:70387–400. http://dx.doi.org/10.1109/ACCESS.2020.2986537.

[17] Guo Haifeng, Wang Kai, Cui He, Xu Aidong, Jiang Jin. A novel method of fault detection for solenoid valves based on vibration signal measurement. In: 2016 IEEE international conference on internet of things (IThings) and IEEE green computing and communications (GreenCom) and IEEE cyber, physical and social computing (CPSCom) and IEEE smart data. 2016, p. 870–3. http://dx.doi.org/10.1109/iThings-GreenCom-CPSCom-SmartData.2016.179.

[18] Li Shou, Liu Xin, Liu Weirong, Rong Mi, Zhu Zhengfa, Zhou Feng. A remaining useful life estimation method for solenoid valve based on mmwave radar and auxiliary particle filter technique. IEICE Electron Express 2021;advpub. http://dx.doi.org/10.1587/elex.18.20210344.

[19] Filho José Roberto Branco Ramos, Negri Victor Juliano De. Model-based fault detection for hydraulic servoproportional valves. In: 13th scandinavian international conference on fluid power. 2013.

[20] Kulkarni Chetan S, Daigle Matthew, Gorospe George, Goebel Kai. Validation of model-based prognostics for pneumatic valves in a demonstration testbed. In: Annual conference of the prognostics and health management society. 2014.

[21] Vaughan ND, Gamble JB. The modeling and simulation of a proportional solenoid valve. J Dyn Syst Meas Control 1996;118(1):120–5. http://dx.doi.org/10.1115/1.2801131.

[22] Taghizadeh M, Ghaffari A, Najafi F. Modeling and identification of a solenoid valve for PWM control applications. Comptes Rendus Mecanique 2009;337(3):131–40.

[23] Angadi SV, Jackson RL, Choe Song-Yul, Flowers GT, Suhling JC, Chang Young-Kwon, et al. Reliability and life study of hydraulic solenoid valve. Part 1: A multi-physics finite element model. Eng Fail Anal 2009;16(3):874–87. http://dx.doi.org/10.1016/j.engfailanal.2008.08.011, URL https://www.sciencedirect.com/science/article/pii/S135063070800157X.

[24] Mazaev T, Ompusunggu A P, Tod G, Crevecoeur G, Van Hoecke S. Data-driven prognostics of alternating current solenoid valves. In: 2020 prognostics and health management conference. 2020, p. 109–15.

[25] Utah MN, Jung JC. Fault state detection and remaining useful life prediction in AC powered solenoid operated valves based on traditional machine learning and deep neural networks. Nucl Eng Technol 2020.

[26] Knoebel Christian, Wenzl Hanna, Reuter Johannes, Clemens year=2017 Guehmann. A compressed sensing feature extraction approach for diagnostics and prognostics in electromagnetic solenoids. In: Annual conference of the prognostics and health management society 2017, Vol. 9. (1).

[27] Seo Boseong, Jo Soo-Ho, Oh Hyunseok, Youn Byeng D. Solenoid valve diagnosis for railway braking systems with embedded sensor signals and physical interpretation. In: Annual conference of the prognostics and health management society. 2016.

[28] Ompusunggu AP, Hostens E. Physics-inspired feature engineering for condition monitoring of alternating current solenoid-operated valves. In: Fifth international conference on maintenance, condition monitoring and diagnostics. 2021.

[29] Tod G, Mazaev T, Eryilmaz K, Ompusunggu A P, Hostens E, Hoecke S V. A convolutional neural network aided physical model improvement for AC solenoid valves diagnosis. In: 2019 prognostics and system health management conference. 2019, p. 223–7.
[30] Tameson. Choosing an AC or DC solenoid valve coil. 2021, URL https://tameson.com/choosing-an-ac-or-dc-coil-for-a-solenoid-valve.html.
[31] Szente V, Vad J. Computational and experimental investigation on solenoid valve dynamics. In: 2001 IEEE/ASME international conference on advanced intelligent mechatronics. proceedings (Cat. No.01TH8556), Vol. 1. 2001, p. 618–23.
[32] Riba JR, Espinosa AG, Cusido J, Ortega JA, Romeral L. Design of shading coils for minimizing the contact bouncing of AC contactors. In: 2008 proceedings of the 54th IEEE holm conference on electrical contacts. IEEE; 2008, p. 130–6.
[33] Tsai Hsun-Heng, Tseng Chyuan-Yow. Detecting solenoid valve deterioration in in-use electronic diesel fuel injection control systems. Sensors 2010;10(8):7157–69.
[34] Coleman Thomas F, Li Yuying. An Interior Trust Region approach for nonlinear minimization subject to bounds. SIAM J Optim 1996;6(2):418–45. http://dx.doi.org/10.1137/0806023, arXiv:10.1137/0806023.

2023-04-05

An improved first-principle model of AC powered solenoid operated valves for maintenance applications

Tod, Georges

Elsevier

Tod G, Ompusunggu AP, Hostens E. (2023) An improved first-principle model of AC powered solenoid operated valves for maintenance applications. ISA Transactions, Volume 135, April 2023 pp. 551-566

https://doi.org/10.1016/j.isatra.2022.09.032